Proceedings of IMECE'03
2003 ASME International Mechanical Engineering Congress
Washington, D.C., November 15–21, 2003

IMECE2003-42912

NUMERICAL ANALYSIS OF THE CONVECTIVE HEAT TRANSFER IN A COMBUSTOR COOLING JACKET

Gustavo Gutierrez
Mechanical Engineering Department
University of Puerto RicoMayagues, Puerto Rico
00681-9045

Tien-Chien Jen and Tuan-Zhou Yan
Mechanical Engineering Department
University of Wisconsin, Milwaukee
Milwaukee, WI 53211

ABSTRACT

In any combustors and chemical reactors, to achieve high efficiency it is very important to maintain the high gas temperature inside the combustion chamber without significant deterioration of the materials of the walls. Thus, a critical aspect of the design of a combustor or reactor is the development of a method to cool the inner walls of a combustor such that the temperatures on the inner wall are well below the temperature a material can sustain. A typical method to cool a combustor chamber is to use a cooling jacket adjacent to the inner wall of the combustor. In general, the efficiency of this cooling jacket depends on the heat removal capability of the cooling water and the flow channel geometry. It is critically important to control these parameters to enhance the performance of the combustion chamber by decreasing the inner wall temperature below its material limit

This study considers a cylindrical combustor, rotating around its axis. A detailed investigation of the fluid flow and heat transfer processes throughout the cooling jacket is performed. A two-dimensional axial symmetric Navier-Stokes equations and energy equation as a conjugate problem are solved. The flow patterns and temperature distributions of the cooling jacket under the effect of rotation are presented. Also, local friction factor and Nusselt number are calculated along the axial direction.

NOMENCLATURE

Cp : specific heat [J/kg-ºC]
h : heat transfer coefficient [W/m^2-ºC]
k : thermal conductivity [W/m-ºC]
L : length of the combustor [m]
p : pressure [Pa]
r, θ, z : radial, circumferential and axial coordinates
R_0 , R_1 , R_2, R_3 : inner radium of combustor, inner and outer radius of wall of cooling jacket and outer radium wall of combustor, respectively [m].
S_ϕ : source term in the generic property ϕ
V_r , V_θ , V_z : reduced velocities in the r, θ , and z direction respectively [m/s]
T : temperature [ºC]
T_{inn} : inner temperature [ºC]
T_∞ : ambient temperature [ºC]
U_0 : inlet velocity [m/s]

Greek

ρ : density [kg/m^3]
ϕ : generic property
μ : dynamic viscosity [kg/m-s]
Γ : diffusivity for the generic property ϕ
Ω : angular velocity [rad/s]

INTRODUCTION

Fluid flow and heat transfer in annular channel are not only of considerable theoretical interest, but also of great practical importance. An obvious technical application is a rotating combustor where combustion takes place inside it and a water-cooling jacket is used for cool down the wall of the combustor. It is well known that to achieve high efficiency in any combustor and chemical reactor, it is very important to maintain the high gas temperature inside the combustion chamber. Note that the temperatures within the primary zone of a combustor could be significantly higher than the temperatures most materials can withstand. Thus, a critical aspect of the design of a combustor or reactor is the development of a method to cool the inner walls of a combustor such that the temperatures on the inner wall are well below the temperature limit of the material. A cooling jacket adjacent to the inner wall

of the combustor is a typical method to cool a combustor chamber. In general, the efficiency of this cooling jacket depends on the heat removal capability of the cooling water and the flow channel geometry. It is therefore critical to actively control these parameters to enhance the performance of the combustion chamber by decreasing the inner wall temperature below its material limit

This study considers a cylindrical combustor, including a stationary and a rotating combustor, which is a typical structure for internal combustion engines, combustors of external engines such as combustors of MK46, MK48 and Spearfish torpedoes and some chemical reactors. A cooling jacket will be modeled as a concentric cylinder, with water flow in between the inner and outer cylinder wall. The inner cylinder wall is the combustion chamber outer wall. Stationary combustion chamber can be seen as a special case of a rotating combustor with a zero rotational speed. Kuehn and Goldstein [1] provide a detailed review of literature of concentric annular flow. There are many works have been reported in the literature for eccentric cylinders. Only the closely relevant studies are reviewed here. Levy [2] studied experimentally the flow in rotating pipes. Murakami and Kikuyama [3] measured the time-mean average velocity components and hydraulic losses in an axially rotating pipe when a fully developed turbulent flow was introduced into the pipe. Kikuyama *et al.* [4] calculated the velocity distribution in the fully developed region of an axially rotating pipe with the help of a modified mixing length theory proposed by Bradshaw [5]. They assumed the tangential velocity to be a parabolic distribution in the fully developed region, which was further confirmed by their experiments. They found a destabilizing effect of rotation on laminar pipe flow. Reich and Beer [6] studied analytically and experimentally of the effect of tube rotation on the velocity distribution and heat transfer for a fluid flowing inside the tube. Taylor [7] studied the fluid flow stability criteria for circular flow in a concentric rotating cylinder with through flow. By numerically simulating the perturbation equations, the critical Reynolds number, Re=165.76, and the rotational Reynolds number, $\mathrm{Re}_{\varphi} = 53.92$, for the onset of the flow instability were calculated by Mackrodt [8]. If the wall of a non-rotating horizontal pipe, subjected to a small flow rate, is heated, the temperature variations in the fluid cause a secondary flow due to buoyancy forces. Morton [9] investigated this phenomenon and obtained solutions for the velocity and temperature field. Futayami and Mori [10] investigated the laminar mixed convection in a horizontal pipe for ratios of $Gr/Re^2 \cong 1$ by means of an integral method.

All the above-mentioned research work mostly focused on fully developed fluid flow region. However, combustors or chemical reactors are often short, and the flow field and thermal field are most likely under developing conditions within the length of the channel. Since the flow channels in the radial direction are often small in comparison to other two directions (i.e., θ and x), the free convection is not very important in comparison with forced convection. In this paper, the effect of rotation on the velocity and temperature distribution will be investigated. The peripherally averaged friction factor and Nusselt number of a water-cooling jacket in the axial direction are presented.

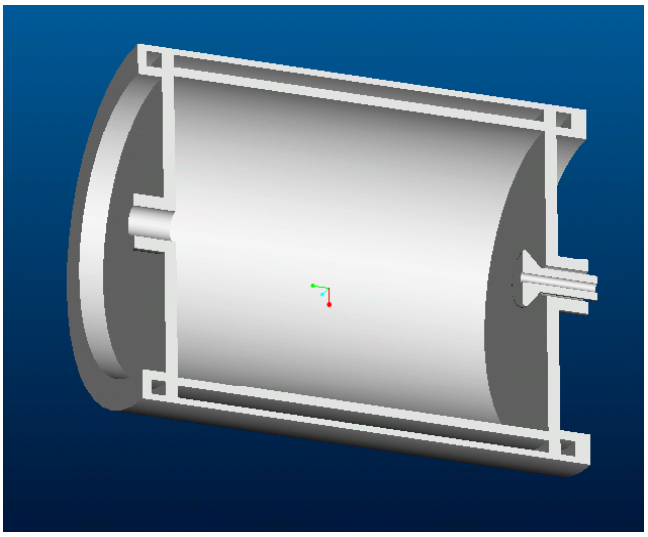

Fig. 1 General structure of combustor

THE PHYSICAL MODEL

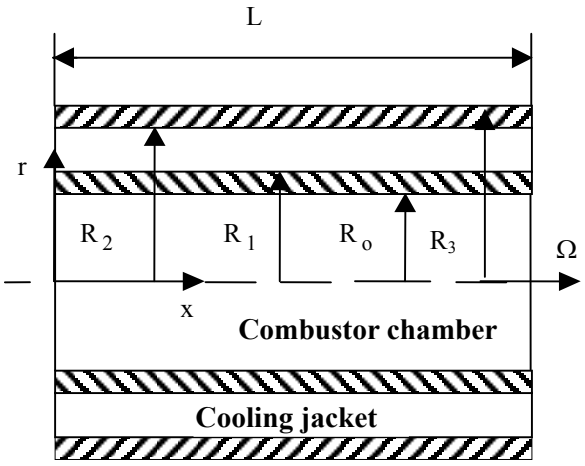

Fig. 2 Physical model and coordinate system

Figure 1 depicts a typical axis-symmetrical combustor. Fuel and oxidant combustion take place inside the combustion chamber. The temperature and pressure inside the combustor are usually very high. To minimize the use of expensive high temperature resistance materials in the hot gas region, the combustion temperature is reduced by the addition of a cooling jacket. Cooling water flow through one end of the annular channel enters the cooling jacket and leaves through the other end of the annular channel at a higher temperature. It is

assumed that the fluid flow is incompressible, steady, laminar flow with constant property. A uniform axial velocity U_0 is assumed at the inlet condition with a constant temperature of T_0. Carbon steel is assumed for the material of the combustor walls. Basic geometric configuration and thermophysical parameters of the combustor under analysis are summarized in Table 1. Note that the Reynolds number based on hydraulic diameter is equal to 468, so the flow is laminar for this analysis.

Figure 2 shows the physical configuration of the combustion chamber, the solid walls and the cooling jacket. The combustor rotates around its axis with an angular velocity Ω (rad/s).

Table1: Basic geometric configuration and thermophysical parameters of the combustor

R_0	50 mm	L	200 mm
R_2	57 mm	U_0	0.05 m/s
R_1	53 mm	Cp_s	434 J/kg-K
R_3	60 mm	Cp_l	4179 J/kg-K
ks	60 W/m-K	μl	0.000855 kg/m-s
kl	0.613 W/m-K	h	10 W/m2-K
ρs	7854 kg/m3	*Tinn*	250 ºC
ρl	1000 kg/m3	*Tamb*	25 ºC

MATHEMATIC FORMULATION

Considering the circumferential symmetry on geometry and boundary conditions, the problem becomes axis-symmetric. In axis-symmetric problems in cylindrical coordinates, all derivatives with respect to the circumferential direction are zero, and the three velocity components are only function of the axial and radial coordinates (x and r). Then, it makes sense to work in cylindrical coordinates rather than Cartesian ones. However, for swirling flows, the circumferential momentum equation has to be solved as well. The choice of the reference frame, inertial or non-inertial, is irrelevant from theoretical point of view. Shifting from one coordinate system to another requires just include the Coriolis acceleration in the source term of equations momentum equation and setting the circumferential velocity $V_\theta = \Omega \times r$ as the no-slip condition. But, for numerical purpose it is convenient to formulate the problem in the non-inertial frame, so the circumferential boundary condition is easily imposed as zero velocity (no-slip condition) at the wall. This is convenient if the problem is solved as a conjugate problem. Viscous dissipation as well as buoyancy effects are assumed negligible.

The governing equations in cylindrical coordinates in the non-inertial frame take the following form:

Mass conservation
$$\frac{1}{r}\frac{\partial}{\partial r}(rV_r)+\frac{\partial V_x}{\partial x}=0 \tag{1}$$

Axial momentum equation
$$\frac{1}{r}\frac{\partial(\rho r V_x V_r)}{\partial r}+\frac{\partial(\rho V_x V_x)}{\partial x}=-\frac{\partial p}{\partial x}+ \mu\left(\frac{1}{r}\frac{\partial}{\partial r}(r\frac{\partial V_x}{\partial r})+\frac{\partial^2 V_x}{\partial x^2}\right) \tag{2}$$

Radial momentum equation
$$\frac{1}{r}\frac{\partial(\rho r V_r V_r)}{\partial r}+\frac{\partial(\rho V_r V_x)}{\partial x}=-\frac{\partial p}{\partial r}+ \mu\left(\frac{1}{r}\frac{\partial}{\partial r}(r\frac{\partial V_r}{\partial r})+\frac{\partial^2 V_r}{\partial x^2}-\frac{V_r}{r^2}\right)+\frac{\rho V_\theta^2}{r}+2\rho\Omega V_\theta \tag{3}$$

Momentum equation in the circumferential direction
$$\frac{1}{r}\frac{\partial(\rho r V_\theta V_r)}{\partial r}+\frac{\partial(\rho V_\theta V_x)}{\partial x}= \mu\left(\frac{1}{r}\frac{\partial}{\partial r}(r\frac{\partial V_\theta}{\partial r})+\frac{\partial^2 V_\theta}{\partial x^2}-\frac{V_\theta}{r^2}\right)-\frac{\rho V_r V_\theta}{r}-2\rho\Omega V_r \tag{4}$$

Energy equation
$$\frac{1}{r}\frac{\partial(\rho r V_r T)}{\partial r}+\frac{\partial(\rho V_x T)}{\partial x}=\frac{\mu}{\mathrm{Pr}}\left(\frac{1}{r}\frac{\partial}{\partial r}(r\frac{\partial T}{\partial r})+\frac{\partial^2 T}{\partial x^2}\right) \tag{5}$$

Where *Pr* is the Prandt number, $\mathrm{Pr}=\frac{c_p\mu}{k}$. The boundary conditions are:

$$r=R_1;\quad V_r=V_x=V_\theta=0;\quad k_l\left.\frac{\partial T}{\partial r}\right|_{r=R_1}=k_s\left.\frac{\partial T}{\partial r}\right|_{r=R_1} \tag{6}$$

At
$$r=R_2;\quad V_r=V_x=V_\theta=0;\quad k_l\left.\frac{\partial T}{\partial r}\right|_{r=R_2}=k_s\left.\frac{\partial T}{\partial r}\right|_{r=R_2} \tag{7}$$

At the entrance of the cooling jacket ($R_1 \le r \le R_2$):
$$x=0;\ V_r=0,\ V_\theta=\Omega r;\ V_x=V_o;\ T=T_o \tag{8}$$

At the outlet of the cooling jacket: $\frac{\partial V_x}{\partial x} = 0$

Temperature of the combustor inner wall is often measured or calculated. Here, it is assumed a constant value of T_{inn}. Convection heat transfer coefficient of the outer wall of the combustor is assumed to be h_o, and the ambient temperature as constant T_∞. At the exit of the cooling channel an outflow boundary condition is used for the momentum equations and an insulated boundary condition is used for the energy equation.

NUMERICAL MODELING

For numerical purpose, it is useful to work with a generic conservation equation, from which the conservation of mass, momentum and energy can be obtained. This generic conservation equation in cylindrical coordinates can be written as:

$$\frac{1}{r}\frac{\partial(\rho r V_r \phi)}{\partial r} + \frac{\partial(\rho V_x \phi)}{\partial x} = \Gamma\left(\frac{1}{r}\frac{\partial}{\partial r}(r\frac{\partial \phi}{\partial r}) + \frac{\partial^2 \phi}{\partial x^2}\right) + S_\phi \quad (9)$$

where ϕ is a generic property, Γ is the diffusivity for the generic property ϕ, S_ϕ is the source term.. It can be seen from Table 2 that one can reproduce the governing equations from this generic equation. The main advantage of the generic conservation equation is that one has to deal with only one equation of the same form in the development of the numerical code. Note that the pressure gradient is included in the source term just for convenience in the formulation. However, in actual computation, this term is treated separately since the pressure field has to be calculated as part of the solution. A pressure correction (or pressure equation) is derived from the momentum equation to enforce mass conservation. The SIMPLEC algorithm is used here [11]. The discretization in cylindrical coordinates generates additional coupling between the momentum equations (i.e., in the S_ϕ term) as shown in Table 2. These terms are treated as extra body forces including the Coriolis force terms (i.e., $2\rho\Omega V_\theta$ and $2\rho\Omega V_r$). The term $\rho\frac{V_r V_\theta}{r}$ in the θ-momentum equation is treated implicitly when the contribution of this term to the central coefficient in the discretized equations is positive, which may reduce the diagonal dominance of the coefficient matrix. This may cause numerical instability of the solution scheme. Otherwise, these terms are treated explicitly. The terms $\mu\frac{V_r}{r^2}$ and $\mu\frac{V_\theta}{r^2}$ in the radial and circumferential momentum equations are treated implicitly as part of the central coefficient.

Table 2-Terms in the generic conservation equation

ϕ	Γ	S_ϕ	Equation
1	-	0	continuity
V_r	μ	$-\frac{\partial p}{\partial r} + \rho\frac{V_\theta^2}{r} + 2\rho\Omega V_\theta$	r-momentum
V_θ	μ	$-\rho\frac{V_r V_\theta}{r} - 2\rho\Omega V_r$	θ-momentum
V_x	μ	$-\frac{\partial p}{\partial x}$	x-momentum
T	$\frac{\mu}{\mathrm{Pr}}$	0	energy equation

The problem can be solved as a conjugate problem assigning a large number to the central coefficient in the solid region (the inner wall and the outer wall). This forces the algorithm to give a zero velocity in the wall regions. This is not advantageous for the solution of the momentum equations but it is very convenient for the solution of the energy equation in which the boundary conditions are unknown in the cooling jacket walls. Another alternative is to solve the flow in the water channel and "inject" the hydrodynamics solution to the conjugate domain. This approach shows a better convergence performance and is used here. Formulating the problem as a conjugate problem, the temperatures at the interfaces are obtained as part of the solution.

CONVERGENCE CRITERIONS AND GRID CONVERGENCE TESTS

The grid convergence tests have been performed as shown in Table 3. In these tests, a rotational speed of 15 rad/s was chosen to ensure that the grid is sufficient to capture the effect of rotating on the cooling jacket flow and heat transfer. A denser grid was used near the entrance, and less dense grid was used next the outlet. The expansion coefficient used in this study is 1.1. In the table, three different grid sizes are tested in radial direction and axial direction; they are16×120, 20×180, and 24×240. The axial velocities were checked at two locations, x=0.1 m, r=0.0545m and x=0.185m, r=0.0555m. It can be seen from the table that the velocities are essentially the same using any of these three grid sizes. The local friction factor and Nusselt number are also compared at x=0.1m, and

similarly, the variation in the calculated results are negligible. After these grid independent tests, a grid of 24 × 240 nodes was used to ensure the highest accuracy of the computational results, and will be used for all the analysis in this paper.

Table 3. Computational test

Grids	16×120	20×180	24×240
u at Ω=15 rad/s x=0.1 r=0.0545	0.037407750	0.037407723	0.037407738
u at Ω=15 rad/s x=0.185 r=0.0555	0.076540340	0.076540341	0 .076540339
f at Ω=15rad/s X=0.1m	0.064618780	0.064618775	0.064618778
Nu at Ω=15rad/s X=0.1	13.26680256	13.26680242	13.26680236

RESULTS AND DISCUSSION

In the discussion that follows, axial velocity profiles and local friction factor at different rotating speeds and different axial locations are examined closely. The effect of this developing flow on temperature distribution and consequently on the Nusselt number is also discussed.

Figure 3 shows the axial velocity flow in the cooling channel without rotation. A uniform input velocity of 0.05 m/s is assumed at the flow inlet boundary. Axial velocity profiles are plotted at four different axial locations. It can be seen that near the entrance at x=0.003, the axial velocity is still fairly uniform at the core of the channel where viscous effects due to the existence of the walls are still not felt. At further downstream locations of x=0.01 and 0.02, the viscous effects penetrate to the center of the annular channel, the velocity profile becomes more parabolic and finally in the fully developed region, x=0.18, it is essentially a parabolic flow profile. The maximum velocity is 0.075 m/s, which equals 1.5 times of the inlet velocity (0.05m/s). This result is in excellent agreement with the exact solution for concentric annular flow. The numerical code was further validated against the exact solution for an annular flow without rotation in the fully developed flow region.

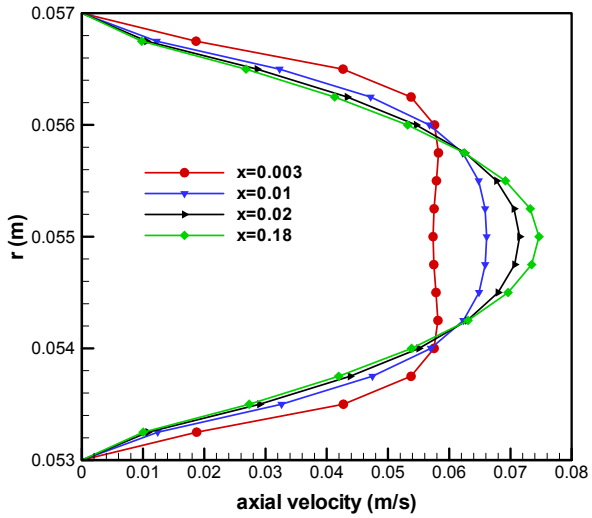

Fig 3. Velocity distribution without rotation

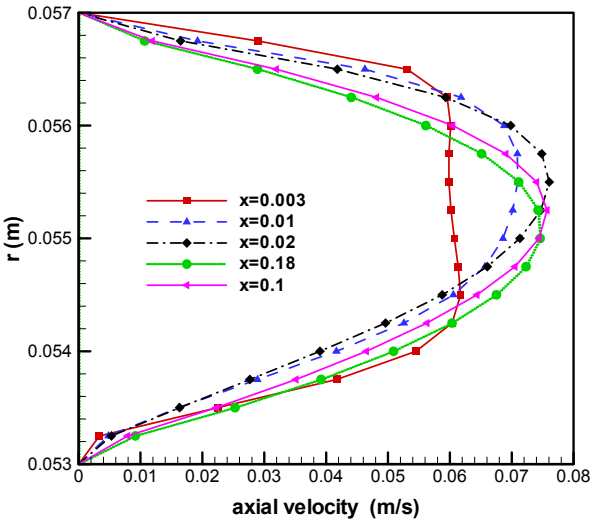

Fig. 4.Velocity distribution with rotation speed of 5 rad/s

Figure 4 shows axial velocity profiles at four different axial locations, similar to Figure 3, for a rotating speed of 5 rad/sec. Since the rotating coordinate is used in this study, the initial velocity field in the θ direction is assumed to be $\Omega \times r$ due to the rotating effect on the flow field. Due to the centrifugal effects, maximum velocities move toward the outer cylinder wall. For a rotating speed of 5 rad/sec, the rotation effect on the flow field is not very significant. However, it can be seen from the figure that the axial velocity profiles are pushed toward the outer wall of the concentric cylinders. Stronger rotating effect on the axial velocity profiles is observed near the entrance, and this effect diminishes near the fully developed region. This is because stronger viscous effect in the fully developed flow region. Figure 5 shows axial velocity profiles at four different axial locations for a higher rotating speed of 10 rad/sec. It can be seen for this rotating speed, a strong recirculating flow next to the entrance with a

maximum negative velocity of approximately –0.02 m/s at x=0.003 m. Moving along the axial direction, this recirculation disappears near x=0.05m (not shown). As can be seen from the figure, this flow reversal phenomenon does not exist at exit at this rotating speed.

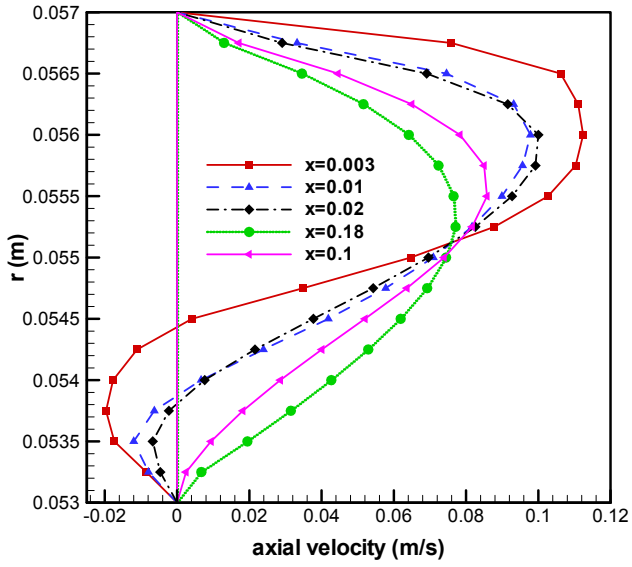

Fig 5.Velocity distribution with rotation speed of 10 rad/s

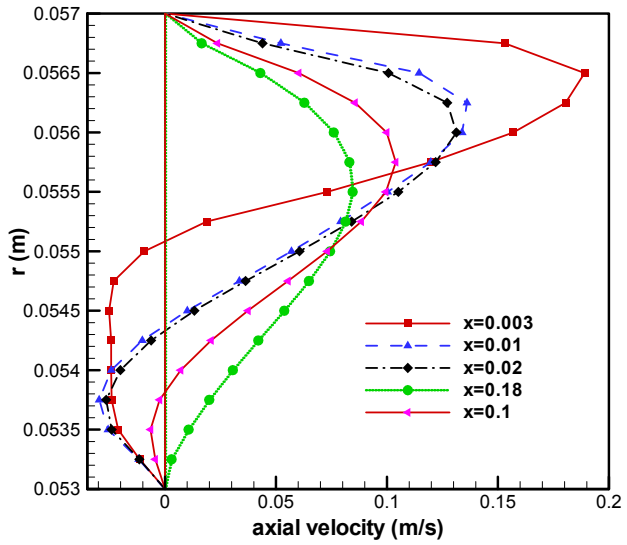

Fig 6. Velocity distribution with rotation speed of 15 rad/s

Figures 6 and 7 show axial velocity profiles at four different axial locations for rotating speeds of 15 rad/sec and 20 rad/sec. It can be observed that the recirculating flow penetrate further into the channel and at Ω=20 rad/sec, negatives velocities start to appear even at the exit. To avoid ill-posed conditions at the outlet boundary, the computational domain was made long enough to assure the exit location was moved downstream from the reattachment point, for the range of rotating speed being analyzed. A channel of 0.4 m was used for all the cases with rotation. However, within the domain of interest, L=0.2 m, the same number of grid nodes was used. It can be observed in these two figures that the shifting of the maximum velocity due to the rotating effect become eminent, even at fully developed flow region. The location of the maximum velocity has shifted from r=0.055 of Ω =0 to r=0.0557 at Ω= 20 rad/s.

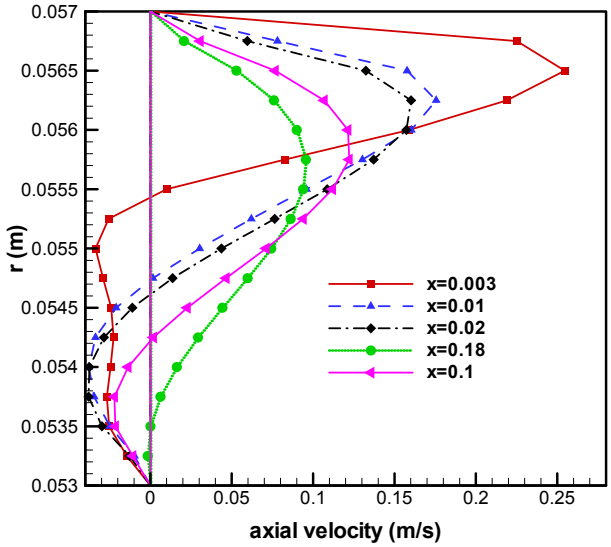

Fig 7. Velocity distribution with rotation speed of 20 rad/s

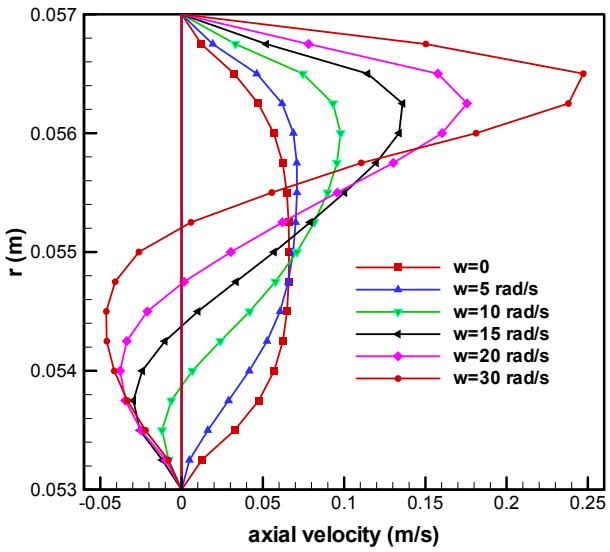

Fig 8. Velocity distribution at x=0.01 m with different rotating speed

Figure 8 shows axial velocity profiles at x=0.01 m for all five different rotating speeds, Ω= 0, 5 rad/s, 10 rad/s, 15 rad/s and 20 rad/s. It is clearly shown in this figure that how the recirculation flow penetrates into the channel when rotating speeds increase. It is also observed that maximum and reverting

velocities (negative velocities) moves inward for increasing rotating speeds.

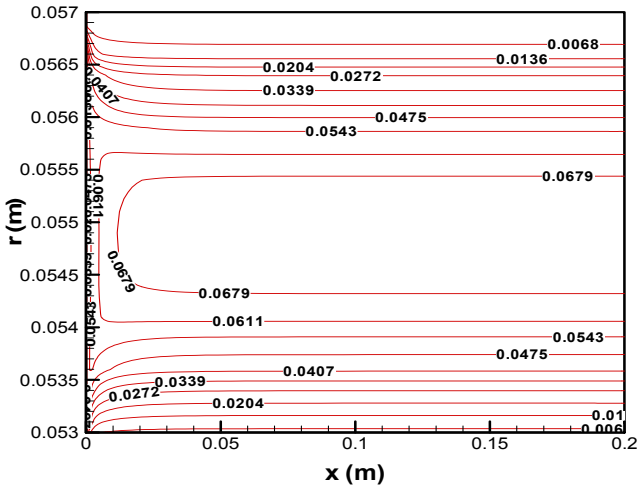

Fig 9. Axial isovel pattern without rotation

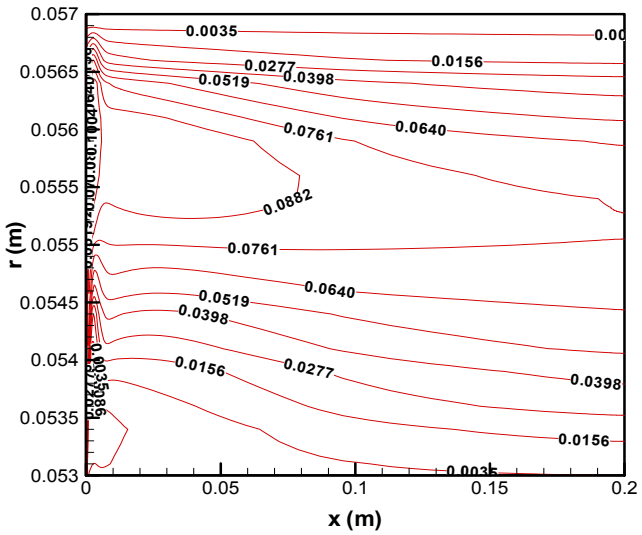

Fig 10. Axial isovel pattern with rotational rate=10 rad/s

Figures 9 to 12 show the axial isovel (constant axial velocity lines) patterns for the rotational speed 0, 10, 20 and 30 rad/s. When the rotational speed is 0 as shown in Figure 9, it can be seen that there is a fairly symmetric isovel pattern along the center of the channel. As the rotational speed increases to 10 rad/s as shown in Figure 10, a small size re-circulating flow is formed near the inlet (not clearly seen in this figure), and a larger velocity gradient is seen near the outer wall, which is consistent with Figure 8. When the rotational speed increases over 10 rad/s as shown in Figures 11 and 12, negative isovel cell can be seen clearly near the entrance. The sizes of the re-circulating flow regions become larger as the rotating speed increases. Again, it is seen from Figure 12 that at Ω = 30 rad/s, the re-circulating flow essentially occupies the entire axial distance of the cooling jacket.

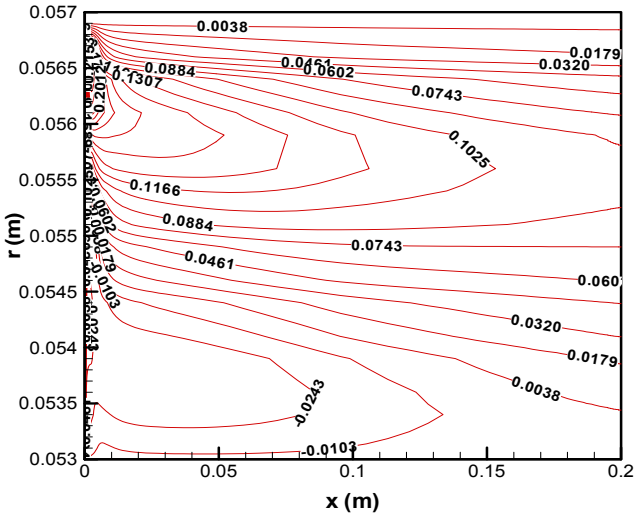

Fig. 11. Axial isovel pattern with rotational rate=20 rad/s

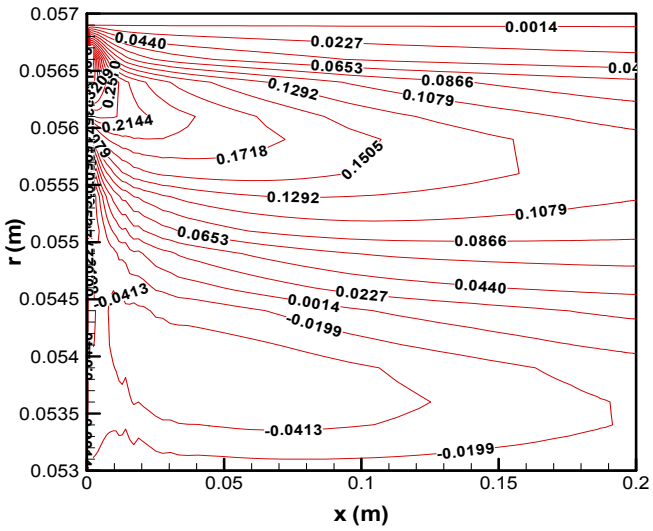

Fig. 12 Axial isovel pattern with rotational rate=30 rad/s

Figures 13, 14 and 15 show the isothermal pattern for three different rotating speeds, Ω =, 0 rad/s, 10 rad/s, and 20 rad/s, respectively. It can be seen very clearly that a strong temperature penetration as the rotating speed increases. This indicates that the higher the rotating speed, the higher the heat transfer rate, which is favorable in the temperature control of the combustor wall. It is worth noting that in Figure 15, the

existence of the flow re-circulating region, has further increased the heat penetration toward the fluid.

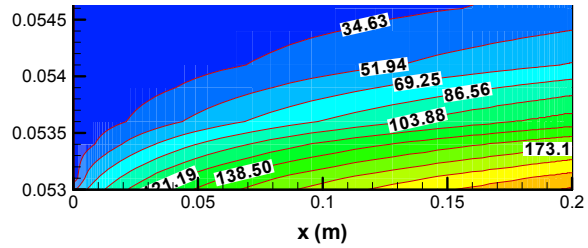

Fig. 13 Isothermal pattern without rotation

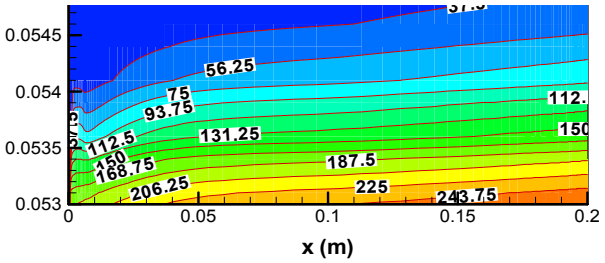

Fig. 14 Isothermal pattern with rotational rate=10 rad/s

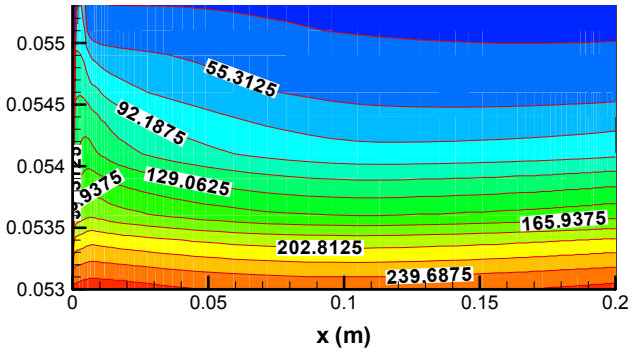

Fig. 15 Isothermal pattern with rotational rate=20 rad/s

Figure 16 shows the friction factor as a function of the local axial locations. This friction factor was defined based on an average pressure calculated at each cross section along the axial direction, as follow:

$$f = \frac{-\left(d\overline{P}/dx\right)D_h}{\rho U_0^2/2} \qquad (10)$$

where $\overline{P} = \frac{2}{\left(R_2^2 - R_1^2\right)}\int_{R_1}^{R_2} P\, r\, dr$, and the hydraulic diameter $D_h = 2\left(R_2 - R_1\right)$. As can be seen the friction factor increases with the rotating speed and reaches a practically constant value near the exit except for Ω=30 rad/sec, which is still developing. The average pressure drop can be calculated by integrating the friction factor along the axial coordinate. However, as can be seen from the figure, the friction factor is almost constant along the channel except for a short distance (for x<0.02) from the entrance, which does not contribute much to the pressure drop. For practical application purpose, a constant friction factor can be estimated from the figure to calculate the pressure drop along the cooling jacket.

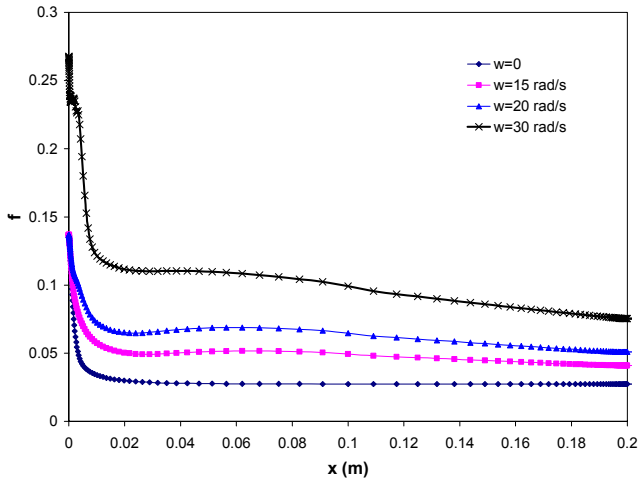

Fig. 16 Friction factor along axial direction

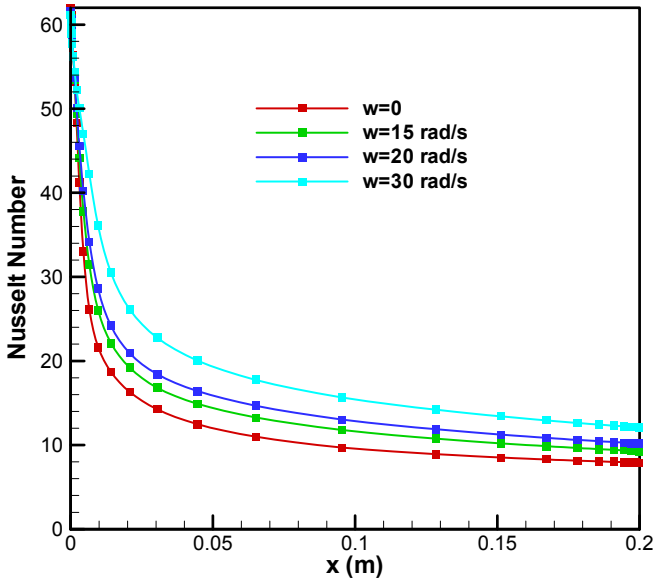

Fig. 17 Nusselt number along axial direction

Figure 17 shows the internal Nusselt number as a function of the axial coordinate. This Nusselt number was computed based on the heat transfer rate at the inner wall. It can be seen that the temperature field is under developing conditions. For Ω=0 (flow without rotation), the Nusselt number for an annular flow at fully developed condition agrees with the exact solution

(see, e.g., Kays and Perkins (1985) and Reich and Beer (1989)). For increasing rotating speeds a noticeable increase in the Nusselt number can be observed. Note that the entire channel is still under thermally developing condition due to the short channel length. Rotating effects retards the establishment of the thermal fully developed region, providing higher Nusselt numbers and consequently higher heat transfer coefficient and better cooling performance.

Conclusions

A numerical analysis of the cooling jacket of a cylindrical combustor, rotating around its axis was carried out. The cooling jacket was modeled as a two-dimensional axial symmetric problem. Navier-Stokes equations and energy equation as a conjugate problem were solved. The flow and heat transfer processes throughout the cooling jacket were addressed.

For a rotating channel, a recirculating flow generates next to the entrance and penetrates further into the channel as rotating speeds increase. Due to centrifugal effects, maximum velocities move toward the outer cylinder wall. In the presence of negatives velocities in recirculating flows, magnitude of maximum velocities increase due the mass conservation requirement.

Friction factor increases with increasing rotating speeds. However, for practical application purpose a constant friction factor can be used to calculate the pressure drop along the cooling jacket.

For increasing rotating speeds a noticeable increase in the Nusselt number was observed. Rotating effects retards the establishment of the thermal fully developed region, providing higher Nusselt numbers and consequently higher heat transfer coefficient and higher heat transfer rate for cooling performance.

Acknowledgement

Dr. Gustavo Gutierrez appreciates the support of University of Puerto Rico-Mayaguez for this work. Dr. Tien-Chien Jen and Mr. T. Z. Yan would like to thank UW System Applied Research for their financial support of the project.

References

[1] T. H. Kuehn and R. J. Goldstein, An experimental and theoretical study of natural convection in the annulus between horizontal concentric cylinders, *J. Fluid Mech.* **74**, 695-719 (1976)

[2] F. Levy, *VDI Forschungsarbeiten auf dem Gebiet des Ingenieurwesens* **32**, 18 (1929)

[3] M. Murakami and K. Kikuyama, *J. Fluids Eng.* **102**, 97 (1980)

[4] K. Kikuyama, M. Murakami, K. Nishibori and K. Maeda, *Bull. JSME* 26, 506 (1983)

[5] P. Bradshaw, *J. Fluid Mech.* **36**, 177 (1969)

[6] G. Reich and H. Beer, *Int. J. Heat Mass Transfer* **32**, 551(1989)

[7] G. I. Taylor, Satbility of a viscous liquid contained between two rotating cylinders. *Phil. Tran. R. Soc. (London) **A223**, 289-343 (1923).*

[8] P. A. Machrodt, Stability of Hagen-Poiseuille flow with superimposed rigid rotation. *J. Fluid Mech.* **73**, 153-164 (1976)

[9] B. R. Morton, Laminar convection in uniformly heated horizontal pipes at low Rayleigh numbers, *Q. J. Mech. Appl. Math.* **12**, 410-420 (1959)

[10] K. Futayami and Y. Mori, Forced convection heat transfer in uniformly heated horizontal tubes-theoretical study, *Int. J. Heat Mass Transfer* **10**, 1801-1813 (1966)

[11] Van Doormal, J.P. and Raithby, G.D., Enhancements of the SIMPLE Method for Predicting Incompressible Fluid Flows, *Numerical Heat Transfer*, 7, 147-163 (1984).

[12] W. M. Kay and H. C. Perkins, in W.M. Rohsenow, J. P. Hartnett and E. N. Ganic, Eds., Handbook of Heat Transfer, Fundamentals, Chap. &, McGraw-Hill, New York (1985).